Oxygen extraction from lunar dry regolith: thermodynamic numerical characterization of the carbothermal reduction

Ivan Troisi[1], Paolo Lunghi[2], Michéle Lavagna[3]

Politecnico di Milano, Department of Aerospace Science and Technology, via La Masa, 34, 20156 Milano, Italy

Abstract

In Situ Resource Utilization constitutes an enabling technology for future, long-term human space exploration. The potentiality of oxygen extraction from dry lunar regolith by means of carbothermal reduction is analyzed in this work. Focus is placed on the scarcely investigated temperature range 1273–1373 K, looking at the possibility to operate below the regolith melting point. The first aspect to consider is to properly identify candidate species and reaction paths that can lead to oxides reduction. This is achieved by modeling the Gibbs free energy ΔG° trend for suitable reactions, looking at which species can react in the temperature range of interest among the minerals and oxides present in the regolith. A more detailed investigation is presented for the SiO_2 and TiO_2 oxides families, being both particularly attractive: the former for its ubiquitous presence in the lunar soil, the latter for its importance in past ISRU literature and its local peaks of concentration in specific areas on the Moon. Finally, a preliminary indication on the expected contribution of each species

[1]PhD Candidate, Department of Aerospace Science and Technology, Politecnico di Milano, ivan.troisi@polimi.it

[2]Assistant Professor, Department of Aerospace Science and Technology, Politecnico di Milano, paolo.lunghi@polimi.it

[3]Full Professor, Department of Aerospace Science and Technology, Politecnico di Milano, michelle.lavagna@polimi.it

to the total yield is given.

Keywords: In Situ Resource Utilization (ISRU); Moon; Water; Oxygen; Carbothermal reduction; Lunar regolith; Thermodynamic of chemical reactions

1. Introduction

In Situ Resource Utilization [1] comprises a set of enabling technologies for human space exploration. The capability to extract and process local resources would dramatically ease the establishment of long-term outposts, e.g. for the construction of structural elements [2], but also for life consumables and propellant production, in particular water and oxygen. Due to its abundance and ease of harvest and handling, lunar regolith is an ideal candidate as raw material for ISRU. Its major constituent is oxygen [3] that can be utilized for both life support and propellant, the latter together with hydrogen either extracted or brought from Earth. Regolith itself can be used as raw material for 3D printing [4], and even for hybrid rockets construction [5]. The incorporation of ISRU capabilities can provide multiple benefits for exploration activities, as it implies mass, cost and risk reduction, together with increased flexibility [6, 7].

Techniques for oxygen and/or water extraction from lunar regolith were ranked by Taylor and Carrier [8], according to technology readiness, number of steps, process conditions and feedstock requirements. Eight likely candidates were identified. Ranked in decreasing relevance order, they are: vapor pyrolysis; glass reduction with H_2; molten silicate electrolysis; ilmenite reduction with H_2; fluxed molten silicate electrolysis; ion plasma pyrolysis; ilmenite reduction with C/CO; ilmenite reduction with CH_4. Further options were listed, but at that time they were considered too immature and not worthy of further investigation. Nowadays, only some of them are still being considered by main space agencies and the scientific community [9].

This work focuses on oxygen extraction from lunar regolith by means of carbothermal reduction in the thermal range 1273–1373 K, particularly attractive for it avoids the feedstock melting. The handling of a molten phase adds several technological and operational complexities to a plant required to automatically operate on the lunar surface, an already extreme environment [10]. The melting point of the lunar regolith is different across the lunar regions, for it depends on the specific mixture of minerals. A common melting temperature range for lunar highlands is 1423–1573 K [11, 12], implying that the target temperature for the proposed carbothermal reduction reaction is close to the melting point and above the glass transition temperature of the material, usually identified at 2/3 of the melting temperature [12, 13]. The basic reaction for the carbothermal process occurs between carbon and most of the metal oxides contained in the regolith minerals: $\mathrm{MeOx_{(s)}} + \mathrm{C_{(s)}} \longrightarrow \mathrm{CO_{(g)}} + \mathrm{Me_{(s)}}$. The designated carbon carrier is a flux of methane, which as a gas favors the reaction with respect to solid carbon (graphite), and eases the removal of syn-gases from the system, allowing to operate in excess of reactants [14]. Several oxides are sensitive to carbothermal reduction: for ISRU applications, the most interesting species to reduce is $\mathrm{SiO_2}$, the most abundant in all the lunar regions.

The most prominent alternative process considered in literature for ISRU oxygen extraction is reduction by hydrogen: $\mathrm{MeOx_{(s)}} + \mathrm{H_{2(g)}} \longrightarrow \mathrm{Me_{(s)}} + \mathrm{H_2O_{(g)}}$. In the temperature range considered by this work, the main mineral that hydrogen can reduce is ilmenite ($\mathrm{FeTiO_3}$), in particular its ferrous parts [15, 16]. However, the concentration of this mineral in the lunar regolith is greatly uneven, according to the specific location. On average, it constitutes only a small fraction of the feedstock (1–2 %), with peaks up to 20 % in some areas [17], making the efficiency of this process largely dependent on the specific landing site. Conversely, the potential capability of the carbothermal reduction to react with a wide range of minerals makes it potentially

site-independent, a very attractive property for future settling of human permanent outposts. Another method considered in recent years for ISRU is the Fray-Farthing-Chen Cambridge (FFC) process, envisaging a cathode made by lunar regolith in an electrolytic cell with molten $CaCl_2$ at about 933-1223 K. Despite the very high theoretical yield (up to 85-96 % of the available oxygen could be extracted at 1223 K and 40 % at 933 K), many complexities are introduced by this process: handling of a molten phase, issues regarding the efficient removal and re-use of molten salts, anode deterioration, and in-situ production of synthesized regolith tiles as cathode [18, 19].

Given the complex mixture presented by regolith, with uneven reactivity levels, a correct interpretation of experimental results can be hard, for the discernment of the actual reacting species is difficult. This work aims to identify potential candidates species contributing to the carbothermal reduction reaction, among all the compounds which constitute the lunar regolith. This is done by modeling the variation of the Gibbs free energy ΔG° of the most likely reactions among the regolith species, the reducing gases, and the carbon that might be deposited during the process. Thermodynamic models allow the identification of both direct and indirect candidate reaction paths leading to oxygen extraction. Such analysis intends to pave the way for subsequent experimental activities. In fact, actual process performances depend on several factors beyond thermodynamic considerations, like access to oxides inside minerals, diffusion of reactants inside regolith particles, possible local phase changes in single particles, reactants ratio and equilibrium conditions. All these aspects concur to the formulation of a consistent kinetic model, whose parameters can be quantified only in a statistical way, estimated from experimental data. Proper interpretation on these data will require solid underlying theoretical foundations, which this work aims to establish.

The paper is organized as follows: in Section 2 the composition of the main types

of lunar regolith is analyzed in terms of minerals and oxides distribution. The carbothermal reduction process is recalled in Section 3, while the description of the adopted numerical model and the related thermodynamic data library are detailed in Section 4. Section 5 constitutes the core of the paper: first, the general reduction reactions of regolith oxides with carbon and hydrogen are analyzed. Then, a deeper investigation is performed on the reaction involving silica (SiO_2) and titanium oxide (TiO_2): the former for its crucial importance, being the most abundant oxide in the lunar regolith and being its reduction path not obvious; the latter for its prominence among past ISRU literature, and its relative abundance in specific lunar regions. Finally, a preliminary estimation of attainable yields for different lunar soils is done: the species included are the ones found to be reactive in the previous sections. In particular, for the silicates is also used the data obtained during an antecedent preliminary thermogravimetric analysis on small quantities of simulant. Conclusions are drawn in Section 6.

2. Characterization of the lunar regolith

The term *regolith* generally describes the layer or mantle of fragmental and unconsolidated rock material of highly varied character, that nearly everywhere forms the surface of the land and overlies the underlying bedrock on the Moon. It has a mean grain size of 60–80 µm in a 40–800 µm range [20], and it constitutes the primary feedstock available for ISRU on the Moon.

A variety of igneous rock types are present, different not only in their mineral and chemical composition, but also in their relative distribution on the lunar surface. A first big distinction can be done between the dark basalts of the maria and the lighter-colored feldspar-rich rocks of the highlands. Other two notable regions are

the large-scale ejecta ridges and the highlands-mare boundaries (basin margins). In this section, the principal characteristics of the lunar regolith are summarized.

2.1. Mineralogy

The relative proportions of the different kinds of fragments and their mineral compositions are identified. Table 1 reports the basic particle types constituents and their modal proportion: there are mineral fragments, pristine crystalline rock fragments, breccia fragments, glasses of various kinds, and agglutinates. The latter, peculiar of the lunar regolith, are aggregates of smaller soil particles bonded together by vesicular, flow-banded glass [20] generated by meteoric impacts.

Specific minerals forming these particles are identified. Species that can be considered as feedstock material for the carbothermal reduction process are:

- **Silicate minerals.** Pyroxene $[(\mathrm{Ca,Fe,Mg})_2\mathrm{Si}_2\mathrm{O}_6]$, plagioclase feldspar $[(\mathrm{Ca,Na})(\mathrm{Al,Si})_4\mathrm{O}_8]$ and olivine $[(\mathrm{Mg,Fe})_2\mathrm{SiO}_4]$ are the most abundant. Pure silica minerals like quartz are rare on the Moon.

- **Oxide minerals.** The most abundant oxide in the mare basalts is ilmenite $[(\mathrm{Fe,Mg})\mathrm{TiO}_3]$, followed by spinel, that actually has a complex series of solid solutions: $\mathrm{FeCr}_2\mathrm{O}_4$ (Chromite), $\mathrm{MgAl}_2\mathrm{O}_4$ (Magnesium Aluminate), $\mathrm{MgFe}_2\mathrm{O}_4$ (Magnesioferrite); $\mathrm{Fe}_2\mathrm{TiO}_4$ (Ulvospinel); $\mathrm{FeAl}_2\mathrm{O}_4$ (Hercynite). Armacolite $[(\mathrm{Fe,Mg})\mathrm{Ti}_2\mathrm{O}_5]$ is also known for its titanium abundance in lunar basalts.

- **Minor minerals.** Native iron, that contains also a small amount of Ni and Co; troilite FeS. They are notable because they attest the highly-reducing, low-oxygen environment under which the lunar rocks formed.

- **Rare lunar minerals.** Apatite $[\mathrm{Ca}_5(\mathrm{PO}_4)_3(\mathrm{OH,F,Cl})]$ on the Moon contain

Table 1: Modal (vol.%) abundance data for particles in the 1000–90 µm size fraction of representative soils from each mission (credits [20]). Soil samples are from Apollo 11 (10084), Apollo 12 (12xxx), Apollo 14 (14163), Apollo 15 (15xxx), Apollo 16 (6xxxx), Apollo 17 (7xxxx), Luna 16 (21000 and 22001), and Luna 24 (24999).

	10084	12001	12033	14163	15221	15271	64501	67461	72501	76501	78221	21000	22001*	24999
Mineral Fragments														
Pyroxene + Olivine	4.2	18.3	26.3	2.6	16.1	13.5	1.0	0.5	5.2	17.3	9.8	6.4	8.9	40.2
Plagioclase	1.9	3.9	9.9	5.1	13.1	7.4	32.1	12.2	10.9	15.2	9.9	1.1	14.7	10.6
Opaque	1.1	0.2	1.3	—	0.1	0.3	—	1.1	0.1	2.8	0.4	—	0.1	0.2
Lithic Fragments														
Mare basalts	24.0	12.9	7.5	2.2	3.1	3.2	0.3	0.5	2.9	9.2	5.7	18.3	1.7	6.9
ANT†	0.4	1.0	1.3	2.9	2.6	2.2	5.0	21.7	5.2	0.5	2.2	0.8	9.7	3.5
LMB‡	0.8	0.1	0.3	0.3	0.6	0.4	2.1	30.7	2.4	6.3	2.3	0.3	2.8	0.5
Feldspathic Basalt (KREEPY)	1.1	0.5	—	0.6	0.4	1.9	1.6	1.6	0.2	0.2	0.2	1.4	0.8	1.4
RNB/POIK§	—	2.3	3.7	10.9	2.7	2.8	8.3	7.9	9.7	8.1	4.4	2.8	10.9	2.2
Fused Soil Component														
DMB⋆	7.5	9.5	11.9	19.3	13.3	12.9	13.9	11.1	22.6	4.2	12.0	15.0	15.0	10.6
Agglutinate	52.0	40.1	17.0	45.7	36.9	37.0	29.1	8.5	37.6	29.2	46.6	42.8	28.7	16.6
Glass Fragments														
Orange/Black	2.7	0.5	1.5	—	0.4	1.6	0.7	0.5	1.7	1.6	1.6	1.4	0.2	—
Yellow/Green	0.8	2.8	0.2	2.9	4.5	7.0	1.2	—	0.1	1.3	1.3	1.7	0.7	0.9
Brown	—	1.5	7.8	—	0.3	0.3	—	—	0.2	—	—	—	—	0.2
Clear	1.3	1.0	—	1.3	1.5	3.8	1.4	—	0.2	0.8	1.0	2.5	1.1	0.6
Miscellaneous														
Devitrified Glass	1.8	5.0	10.8	6.1	4.1	5.6	3.4	3.2	0.4	2.2	1.9	4.4	4.6	5.4
Others	0.3	0.5	0.5	—	0.3	0.2	—	0.5	0.4	1.1	0.7	1.1	0.1	0.3
Total	99.9	100.1	100.0	99.9	100.0	100.1	100.1	100.0	99.8	100.0	100.0	100.0	100.0	100.1
Number of points	625	823	666	311	1000	1008	942	189	801	820	1266	360	1333	634

* 500–90 µm fraction.
† ANT = anorthosite, norite, troctolite.
‡ LMB = Light matrix breccia.
§ RNB/POIK = Recrystallized noritic breccia/poikilitic breccia.
⋆ DMB = Dark Matrix Breccia

Table 2: Modal proportions (vol.%) of minerals and glasses in soils from the Apollo (A) and Luna (L) sampling sites (90–20 µm fraction, not including fused-soil and rock fragments). (H) denotes highland, (M) denotes mare (credits [17]).

	A-	A-	A-14	A- (H)	A- (M)	A-16	A- (H)	A- (M)	L-16	L-20	L-
Plagioclase	21.4	23.2	31.8	34.1	12.9	69.1	39.3	34.1	14.2	52.1	20.9
Pyroxene	44.9	38.2	31.9	38.0	61.1	8.5	27.7	30.1	57.3	27.0	51.6
Olivine	2.1	5.4	6.7	5.9	5.3	3.9	11.6	0.2	10.0	6.6	17.5
Silica	0.7	1.1	0.7	0.9	-	0.0	0.1	-	0.0	0.5	1.7
Ilmenite	6.5	2.7	1.3	0.4	0.8	0.4	3.7	12.8	1.8	0.0	1.0
Mare Glass	16.0	15.1	2.6	15.9	6.7	0.9	9.0	17.2	5.5	0.9	3.4
Highland Glass	8.3	14.2	25.0	4.8	10.9	17.1	8.5	4.7	11.2	12.8	3.8
Others	-	-	-	-	2.3	-	-	0.7	-	-	
Total	99.9	99.9	100.0	100.0	100.0	99.9	99.9	99.8	100.0	99.9	99.9

F, Cl but no OH, while there are sulfides, phosphides and carbides present in schreibersite [$(Fe, Ni)_3P$], cohenite [$(Fe, Ni)_3C$], and niningerite [$(Mg, Fe, Mn)S$].

The distribution of minerals and oxides across the lunar surface is heterogeneous, and generally dependent on the terrains and the geologic structures. The modal proportions of minerals and glasses in some representative soils are summarized in Table 2.

2.2. Oxides content

For ISRU purposes, the determination of the total oxygen content in regolith is of primary importance. Oxygen constitutes about 40–45 % of the regolith [3]: this fraction varies slightly across the lunar surface, and it is stored in different types of oxides, whose relative distribution is terrain-dependent. Table 3 reports the composition ascertained at the landing sites of three Apollo missions. Apollo 11 (soil 10002) represents the composition of a high-Ti basalt; Apollo 14 and Apollo 16 average compositions, instead, are representative respectively of a mare basalt and a

Table 3: Composition for three representative sites of maria (Apollo 11 and 14) [21] and highlands (Apollo 16) [3]. Values are not normalized to 100 % as the original data.

Oxide	**Apollo 11 (soil 10002)** [%]	**Apollo 14 (average soil)** [%]	**Apollo 16 (average soil)** [%]
$\mathbf{SiO_2}$	42.20	48.10	45.09
$\mathbf{TiO_2}$	7.80	1.70	0.56
$\mathbf{Al_2O_3}$	13.60	17.40	27.18
$\mathbf{Cr_2O_3}$	0.30	0.23	0.11
FeO	15.30	10.40	5.18
MnO	0.20	0.14	0.07
MgO	7.80	9.40	5.84
CaO	11.90	10.70	15.79
$\mathbf{Na_2O}$	0.47	0.70	0.47
$\mathbf{K_2O}$	0.16	0.55	0.11
$\mathbf{P_2O_5}$	0.05	0.51	0.12

lunar highland. In all of them the predominance of silicates is clear: targeting those species could easily make the carbothermal reduction process site-independent.

2.3. Regolith simulants

Given the extreme scarceness of lunar regolith specimens on Earth, the usage of simulant is mandatory to achieve experimental confirmation of ISRU processes. In fact, the availability of lunar material is extremely limited, for all the lunar samples currently on Earth were collected along a few space missions from 1969 to today, for a total mass of less than 400 kg. Lunar regolith simulant is adopted for intensive and destructive test campaigns: according to the different Moon features, it is estimated that a number between five and ten simulant materials would be adequate to describe the main areas [21]. The identification of the differences between sim-

ulant and actual regolith is essential to correctly interpret experimental results and extrapolate performances for actual lunar soil. In particular, it has been found that most of the simulants include iron in the form of Fe_2O_3, normally absent in the real regolith, in which iron is present as FeO [21, 3]. The reactivity of this species shall be taken into account, so it is included in the current analysis. NU-LHT-2M simulant, which matches the modal mineral content and grain-size distribution of the Apollo 16 mission regolith samples [3], was employed at Politecnico di Milano for preliminary experimental tests. This particular simulant is chosen to show more clearly the larger set of active species available to carbothermal reduction with respect to the hydrogen one: indeed this simulant has a low ilmenite content (<1 %) [17]), the mineral that can be reduced with hydrogen, as it is highlighted in the introduction.

3. Process state of the art

Carbothermal reduction is a well-known process exploited on Earth to extract metals, silicon, and their compounds from a feedstock of oxides. In standard plants, the reaction is induced by mixing the feedstock with carbon and then by warming up the mixture at high temperature [22]. In the context of lunar ISRU, different studies are present in literature regarding the carbothermal process on molten regolith, with a temperature higher than 1773 K [10, 23].

This work focuses instead on the carbothermal reduction within the target temperature range from 1273 K to 1373 K, above the glass transition temperature, but still below the melting point. In fact, a liquid, melted phase would add significant layers of complexity in a plant required to operate in autonomy in an extremely severe environment like the lunar surface. Conversely, the maintenance of a solid phase greatly eases feedstock handling, while reducing parts wear and power consumption.

The general chemical mechanism is represented by the reaction:

$$\mathrm{MeO_{(s)}} + \mathrm{C_{(s)}} \longrightarrow \mathrm{CO_{(g)}} + \mathrm{Me_{(s)}} \tag{1}$$

where starting with a generic metal oxide, metal (Me) and carbon monoxide (which constitutes the main oxygen carrier) are obtained. Looking for a closed loop process, carbon to be replaced by methane is here proposed, getting to reaction:

$$\mathrm{MeO_{(s)}} + \mathrm{CH_{4(g)}} \longrightarrow \mathrm{CO_{(g)}} + 2\,\mathrm{H_{2(g)}} + \mathrm{Me_{(s)}} \tag{2}$$

As hydrogen is present in the gaseous reactants mixture, also its reaction with the metal oxide is taken into account in this kind of process:

$$\mathrm{MeO_{(s)}} + \mathrm{H_{2(g)}} \longrightarrow \mathrm{H_2O_{(g)}} + \mathrm{Me_{(s)}} \tag{3}$$

In the temperature range of interest, carbothermal reduction is not yet examined in depth by the existing literature [24]. Indeed, whenever feedstocks rich in silicon are considered, literature shows to be beneficial working at $T > 1573\,\mathrm{K}$ to gain syn-gas products yields in the order of $20 - 30\,\%$ while keeping the time to product short [10]. As reported in Fig. 1, retrieved from [25] and showing a numerical equilibrium analysis of the carbothermal reduction of $\mathrm{SiO_2}$ using commercial software, high temperatures are beneficial in avoiding coke formation, in effectively reducing the silica and maximizing the yield in syn-gases production, formally carbon monoxide [25], but at the price of a melting phase.

In an end-to-end ISRU plant on the lunar surface, the carbothermal reduction would be followed by a methanation stage at lower temperature to convert carbon monoxide and hydrogen into a mixture of water and methane. The reaction, induced by a catalyst at a convenient temperature (around $250\,^{\circ}\mathrm{C}$ [26]) is described by the equation:

$$\mathrm{CO_{(g)}} + 3\,\mathrm{H_{2(g)}} \longrightarrow \mathrm{CH_{4(g)}} + \mathrm{H_2O_{(g)}} \tag{4}$$

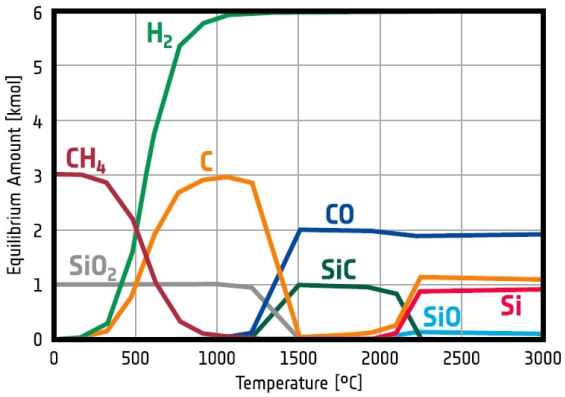

Figure 1: Equilibrium of the carbothermal reduction process on SiO_2 vs temperature (credits [25]).

Water vapor constitutes an oxygen carrier much easier to be handled with respect to CO, and can be easily separated by condensation. Eventually, liquid water can be passed to an electrolysis stage: gaseous oxygen is stored, while hydrogen and methane can be recycled in an ideally perfectly closed loop. Methanation and water electrolysis are very well-known processes: this work focuses on carbothermal reduction only.

4. Thermodynamic model

The aim of this work is the analytical identification of candidate chemical species, inside the lunar regolith, capable to react with the reducing gases H_2 and CH_4 in the temperature range 1273–1373 K. Then, reactions with methane, carbon, and hydrogen are considered.

The trend of the Gibbs free energy (ΔG°) against temperature is analyzed for a set of relevant reactions to detect the $\Delta G^\circ < 0$ interval, in which reactions may naturally occur. Indeed a complete view can be given only by matching these results with the chemical kinetic: the equilibrium among the species can either enlarge or reduce the temperature intervals in which the reactions are possible, close to the

point of $\Delta G^\circ = 0$. Nevertheless, thermodynamic analysis allows identifying all the potential candidates reactions happening in the feedstock mixture. The computation of the ΔG° trend is performed by a custom Python script. In the following, the model adopted is detailed, together with the data sources assumed for the study, and the code validation process.

4.1. Model description

The first step is the formalization of the reactions, that includes the reduction of different minerals and oxides contained in the lunar regolith (as shown in Section 2) with methane, hydrogen and carbon. The reactions considered in this work are detailed in Section 5.

Once a reaction is formalized, the ΔG° trend is computed by means of the Gibbs free energy formulation $\Delta G^\circ = \Delta H^\circ - T\Delta S^\circ$. Both enthalpy and entropy variations ΔH° and ΔS° are temperature-dependent quantities, enabling the evaluation of the free energy along a range of temperatures. The total ΔH° and ΔS° are built summing up all the values of the single ith species in the reaction, pre-multiplying them by the stoichiometric coefficient ν:

$$\Delta H^\circ = \sum_{i=1}^{N_S} \nu_i \Delta H_i^\circ \qquad \Delta S^\circ = \sum_{i=1}^{N_S} \nu_i \Delta S_i^\circ \tag{5}$$

where reactants have a negative integer stoichiometric coefficient, while for products the value is positive. N_S is the number of species in a reaction.

The key expressions that evaluate enthalpy and entropy for each species are polynomials in temperature in the form [27, 28]:

$$\frac{H^\circ(T)}{R_0} = -a_1 T^{-1} + a_2 lnT + a_3 T + a_4 \frac{T^2}{2} + a_5 \frac{T^3}{3} + a_6 \frac{T^4}{4} + a_7 \frac{T^5}{5} + b_1 \tag{6}$$

$$\frac{S^\circ(T)}{R_0} = -a_1 \frac{T^2}{2} - a_2 T^{-1} + a_3 lnT + a_4 T + a_5 \frac{T^2}{2} + a_6 \frac{T^3}{3} + a_7 \frac{T^4}{4} + b_2 \tag{7}$$

where coefficients a_i and b_i are defined for each species and collected in a library (expounded in the next Section). Coefficients are normally identified by experiments: for this reason, for some species different sets of coefficients are defined for different temperature intervals. In addition, for each species a reference temperature T_{ref}, the reference standard enthalpy of formation $\Delta_f H^\circ(T_{\text{ref}})$, and the reference standard molar entropy $S^\circ(T_{\text{ref}})$ are defined as well.

Given a species whose thermodynamics coefficients are defined over n intervals, and a reaction temperature T, the first step in the evaluation is the identification of the active interval in which the current temperature T lies: let this interval be identified by the index $m \leq n$. Direct subtraction of references values from $H_i^\circ(T)$ and $S_i^\circ(T)$ leads to numerical errors, for the trends of enthalpy and entropy are subject to discontinuities across temperature intervals due to possible phase changes. To achieve a correct evaluation of ΔH_i° and ΔS_i°, the subtraction shall be performed for each interval:

$$\Delta H_i^\circ(T) = \Delta_f H_i^\circ(T_{\text{ref}i}) + \sum_{j=1}^{m} \Big(H_i^\circ(T_{1j}) - H_i^\circ(T_{0j}) \Big) \tag{8}$$

$$\Delta S_i^\circ(T) = S_i^\circ(T_{\text{ref}i}) + \sum_{j=1}^{m} \Big(S_i^\circ(T_{1j}) - S_i^\circ(T_{0j}) \Big) \tag{9}$$

where i denotes the species, j the temperature interval for which coefficients are defined. The temperatures T_{1j} and T_{0j} are defined for each interval as:

$$T_{0j} = \max(T_{\text{ref}j},\, T_{\text{lo}j}) \tag{10}$$

$$T_{1j} = \min(T,\, T_{\text{up}j}) \tag{11}$$

where $T_{\text{lo}j}$ and $T_{\text{up}j}$ are respectively the lower and the upper temperature boundaries of the jth interval.

4.2. Thermodynamic data library

A library of the chemical species involved in the process under study has been compiled. For each species not only thermodynamics coefficients a_i and b_i, but also other useful quantities for the estimation of ISRU performances, like the molar mass and phase change temperatures are included. Together with the expansion values, the thermodynamic reference values are also needed, so the reference temperature, the enthalpy of formation and standard molar entropy.

To this end, three main sources have been considered: not all sources report data in the same format. In the following, data storage format and post-processing adopted is summarized, while the source for each species is reported in Table 4:

- *NASA-CEA* [29]: $[T_{\mathrm{lo}}, T_{\mathrm{up}}, a_1, a_2, a_3, a_4, a_5, a_6, a_7, b_1, b_2]$. This is the baseline data shape: all the others are elaborated consequently.

- *NIST* [30]: the enthalpy expansion is in the form $H^o(T) = -ET^{-1} + AT + B\frac{T^2}{2} + C\frac{T^3}{3} + D\frac{T^4}{4}$. The information was converted to $[T_{\mathrm{lo}}, T_{\mathrm{up}}, \frac{E}{R_0}, 0, \frac{A}{R_0}, \frac{B}{R_0}, \frac{C}{R_0}, \frac{D}{R_0}, 0, 0, 0]$ to be included in the library.

- Robie and Waldbaum [31], and Berman [32]: in these cases enthalpy and entropy information is stored in tabular format, instead of interpolating coefficients. A MATLAB® script written on purpose has been implemented to interpolate the table data in a set of polynomial coefficients coherently with the convention adopted in this work. In particular, linear interpolation in the intervals is chosen, leaving only a_3 and b_1 as coefficients in the expansion $[T_{\mathrm{lo}}, T_{\mathrm{up}}, 0, 0, a_3, 0, 0, 0, 0, b_1, 0]$. Linear interpolation is chosen for simplicity and for the possibility to manage the discontinuities coming from phase change with no pre/post processing: the precision is not compromised due to the small intervals available (100 K).

Table 4: Bibliographic sources for thermodynamic data library of each considered species.

Bibliographic source	**Species**
Enthalpy and expansion coefficient from *NASA-CEA* [29]; other from *NIST* [30].	SiO_2, Si, CO, CH_4, H_2, Fe, Fe_2O_3, Al_2O_3, Al, TiO_2, H_2O, C, Ti, Na_2O, Na, MgO, CaO, Ca, Mg, Cr_2O_3, Cr, Mn, K_2O, K, Mg_2SiO_4, $MgAl_2O_4$, $MgTi_2O_5$, Ti_2O_3, SiC, SiO, CO_2, TiC, TiO, P_4O_{10}, P, $Mg(OH)_2$, O_2
NIST [30].	FeO
Robie and Waldbaum [31] (validation with Berman [32], whenever available).	MnO, Fe_2SiO_4, $FeCr_2O_4$, $MgFe_2O_4$, $NaAlSi_3O_8$, $CaAl_2Si_2O_8$, $CaMgSi_2O_6$, $MgSiO_3$
Entropy from Berman [32]; other from Robie and Waldbaum [31].	$FeTiO_3$

Tables of the thermodynamic data are included with this paper as supplementary data.

4.3. Code validation

Given the fact that the values in the library are properly defined, a code validation campaign has been performed by a cross-check with data available in the existing literature for selected reactions:

- ΔG° trend for the formation reaction of some key species: in particular CH_4, CO, SiO, SiO_2 formation reactions from the constitutive elements [31];
- Water splitting reaction: $H_2O_{(g)} \longrightarrow 0.5\,H_{2(g)} + O_{2(g)}$ [33];

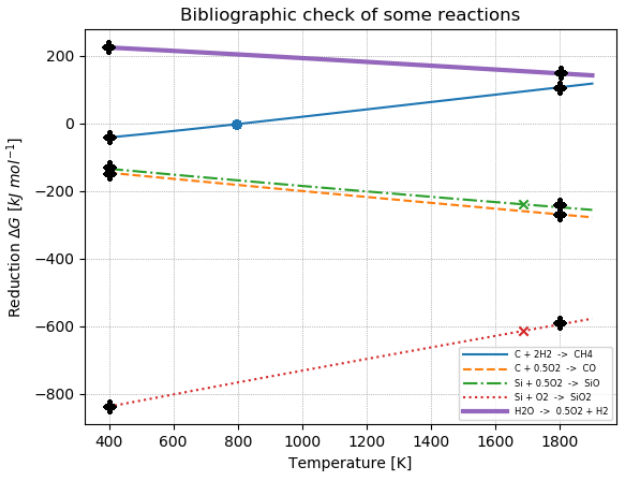

Figure 2: Free energy trend for the formation reaction of CH_4, CO, SiO, SiO_2 and H_2O splitting. The black points are the values coming from [31, 33] for comparison. Reactions: $C_{(s)} + 2\,H_{2(g)} \longrightarrow CH_{4(g)}$; $C_{(s)} + 0.5\,O_{2(g)} \longrightarrow CO_{(g)}$; $Si_{(s)} + 0.5\,O_{2(g)} \longrightarrow SiO_{(g)}$; $Si_{(s)} + O_{2(g)} \longrightarrow SiO_{2(g)}$; $H_2O_{(g)} \longrightarrow H_{2(g)} + 0.5\,O_{2(g)}$.

- Of particular importance for this work, mainly due to the species involved, the reaction of ilmenite with carbon: $FeTiO_3 + C \longrightarrow Fe + TiO_2 + CO$. Compared with the Table 13 in [16], the $\Delta G^\circ = 0$ occurs around 1150 K, exactly the same computed by code. See Fig. 3d, the red line marked with an arrow, superimposed to the $FeCr_2O_4$ one;

- Other notable reactions, whenever data are available in literature, i.e. the reaction $SiO_{2(s)} + C_{(s)} \longrightarrow SiO_{(g)} + CO_{(g)}$ is checked with the trend reported in table IV, page 508 of [34].

Comparisons for formation and water splitting reactions are shown in Fig. 2.

5. Thermodynamic simulation results and discussion

In this section, candidate reactions are formalized and their ΔG° trend with temperature is analyzed. The formulation of the reactions is cross-checked with the available bibliography to ensure the representativeness of the reduction, in particular for the minerals [35, 36, 37, 38, 39, 40]. First, general reductions with methane and carbon (Section 5.1), and hydrogen (Section 5.2) are considered. Then, the investigation is focused on silicon (Section 5.3) and titanium (Section 5.4) oxides, the former for its prominence among the species included in the lunar regolith, the latter for its relative importance in ISRU related literature for comparison purposes. Finally, in Section 5.5 obtained results are exploited to compute a preliminary estimation of the expected yield for different types of lunar soils.

5.1. Reactions with methane and carbon

In the case under examination, carbothermal reduction entails all the reactions between the feedstock and the methane (which is the main carbon carrier), and between the feedstock and solid carbon (which can be formed by methane dissociation in the temperature range of interest). In the following, basic reductions are reported:

Reductions with methane

$$SiO_{2(s)} + CH_{4(g)} \longrightarrow SiO_{(g)} + CO_{(g)} + 2\,H_{2(g)}$$

$$TiO_{2(s)} + 3\,CH_{4(g)} \longrightarrow TiC_{(s)} + 2\,CO_{(g)} + 6\,H_{2(g)}$$

$$MeO_{(s)} + CH_{4(g)} \longrightarrow Me_{(s)} + CO_{(g)} + 2\,H_{2(g)}$$

$$Mineral + CH_{4(g)} \longrightarrow Me_{(s)} + MeOx_{(s)} + CO_{(g)} + 2\,H_{2(g)}$$

Reductions with carbon

$$SiO_{2(s)} + C_{(s)} \longrightarrow SiO_{(s)} + CO_{(g)}$$

$$TiO_{2(s)} + 3\,C_{(s)} \longrightarrow TiC_{(s)} + 2\,CO_{(g)}$$
$$MeO_{(s)} + C_{(s)} \longrightarrow Me_{(s)} + CO_{(g)}$$
$$\text{Mineral} + C_{(s)} \longrightarrow Me_{(s)} + MeOx_{(s)} + CO_{(g)}$$

Reactions are detailed for SiO_2 and TiO_2, while other metal oxides reductions are indicated in a generic form. Oxide species are indicated as generic metal oxides (MeO), the metal with Me, while the decomposed minerals are split in their cation, the metal, and anion, so the oxide, parts. Fig. 3, compares the ΔG° trend against temperature for several species, with methane and carbon. Each reaction can happen at temperatures for which $\Delta G^\circ \leq 0$, marked with a circle placed on each line in the graphs, while the "x" sign marks the phase change occurrence (notably fusion).

It can be noticed that only some of the reactions occur in the range 1273–1373 K, the temperature envelope of interest for the current work. In general, reactions with solid carbon have a $\Delta G^\circ = 0$ temperature higher than the one achieved with methane: this highlights that more energy is required to make the deposited carbon to react with the regolith. It has however to be pointed out a substantial difference between the deposited carbon coming from methane cracking and the adsorbed active carbon. The latter is obtained by the adsorption of the methane, that is dissociated through CH_3, CH_2, CH, and finally $C + 2\,H_2$: its reactivity is higher than graphite, improving the thermodynamics of the process [14].

Furthermore, the obtained results point out the fact that the oxygen trapped in minerals is more difficult to remove with respect to the oxides. For most of the compounds in Fig. 3c–3f, the reaction temperature is generally higher than 1600 K, except for ferrous minerals, that are in the analyzed range (chromite partially overlaps ilmenite). The high reactivity of iron is due to the low free energy of formation of the ferrous compounds, shown also in Fig. 4. The same can be said for some

oxides, like the tetraphosphorus decaoxide (also known in its empirical formula as P_2O_5), TiO_2, Cr_2O_3, Na_2O, K_2O and MnO: they are in the interesting region when reacting with methane, with a little shift to higher temperatures when reacting with carbon.

Summarizing, the species that react with methane and carbon, in the region of interest, are:

- Reaction with CH_4: Fe_2O_3, FeO, TiO_2, Cr_2O_3, MnO, Na_2O, K_2O, P_4O_{10}, (SiO_2) and the minerals Fe_2SiO_4 (fayalite - olivine), $FeTiO_3$ (ilmenite), $FeCr_2O_4$ (chromite - spinel).

- Reaction with C: Fe_2O_3, FeO, K_2O, P_4O_{10}, and the minerals Fe_2SiO_4 (fayalite - olivine), $FeTiO_3$ (ilmenite), $FeCr_2O_4$ (chromite - spinel).

5.2. Reactions with hydrogen

During carbothermal reduction with methane, CH_4 decomposes making available not only carbon but also hydrogen: the presence of the latter in the mixture makes also the reduction with hydrogen theoretically possible. In this reaction, water is produced directly, that is likely to react with the deposited carbon when available. The free energy of the reaction $H_2O_{(g)} + C_s = H_{2(g)} + CO_{(g)}$ can be expressed as $\Delta G^\circ = 133.72 - 0,1419T\,\mathrm{kJ}$, with T expressed in kelvin. The $\Delta G^\circ = 0$ line is crossed at 942 K, producing further CO and contributing to solid carbon removal [42].

In the following, the possible reactions of molecular hydrogen with the same species considered in Section 5.1 are listed:

$$SiO_{2(s)} + H_{2(g)} \longrightarrow SiO_{(g)} + H_2O_{(g)}$$

$$2\,TiO_{2(s)} + H_{2(g)} \longrightarrow Ti_2O_{3(s)} + H_2O_{(g)}$$

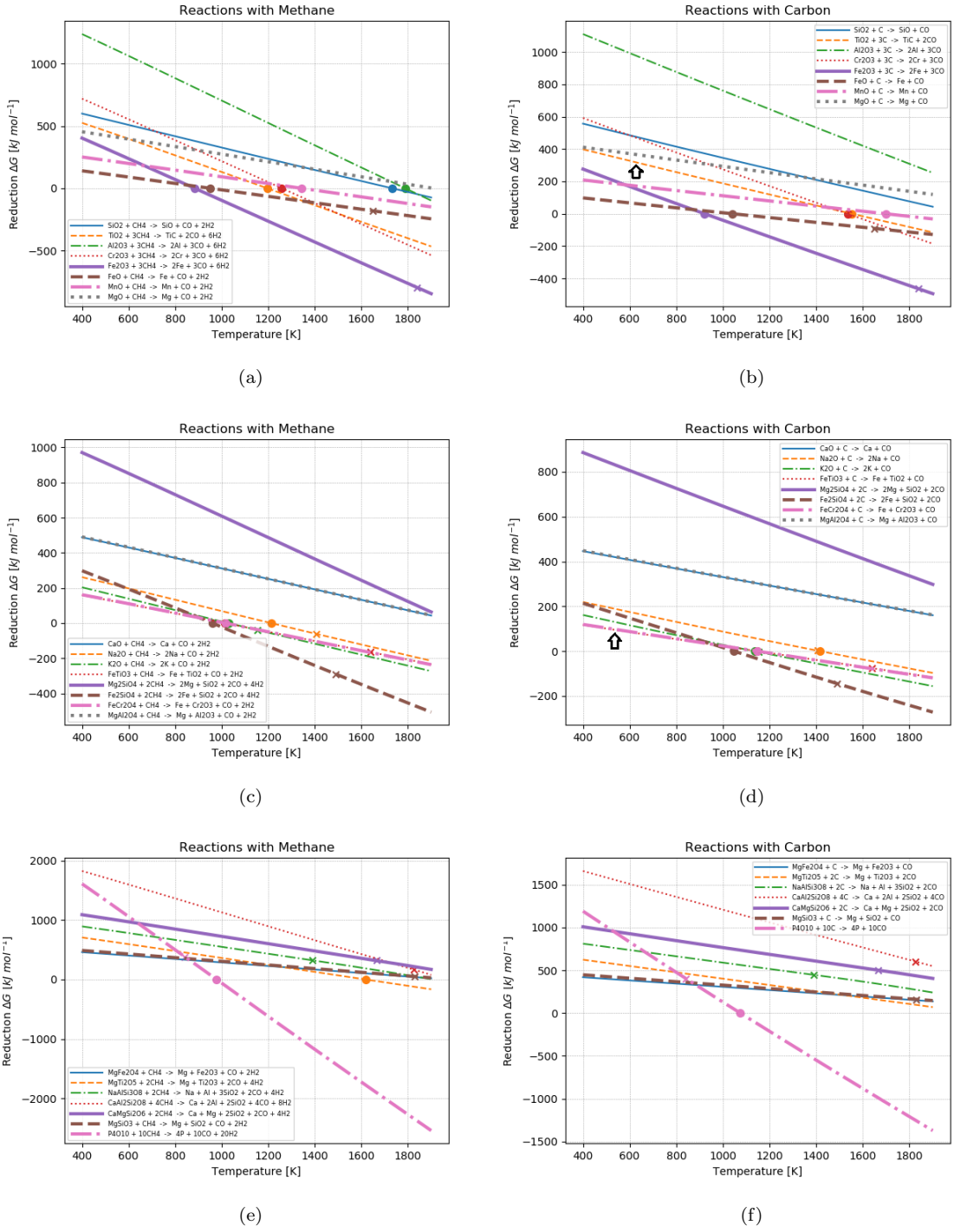

(a) (b)

(c) (d)

(e) (f)

Figure 3: ΔG° behavior of different species for the reaction with CH_4 (left) and C (right). The cross "x" highlights the phase change temperature, the point • indicates the $\Delta G^\circ = 0$ temperature.

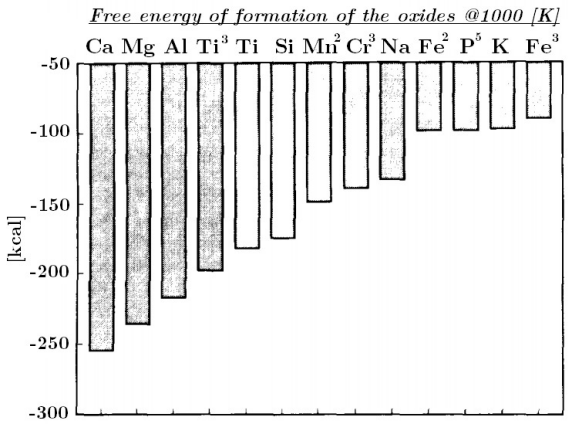

Figure 4: Bar diagram for free energies of formation (kcal per mole of O_2) of lunar-element oxides, 1000 K. Diagram shows affinities of the lunar elements for oxygen (credits [41]).

$$\mathrm{MeO_{(s)} + H_{2(g)} \longrightarrow Me_{(s)} + H_2O_{(g)}}$$
$$\mathrm{Mineral + H_{2(g)} \longrightarrow Me_{(s)} + MeOx_{(s)} + H_2O_{(g)}}$$

In addition, the reaction of hydrogen together with carbon is included:

$$\mathrm{C_{(s)} + 2\,H_{2(g)} \longrightarrow CH_{4(g)}}$$

Results are reported in Fig. 5. It can be noted how the reaction between hydrogen and carbon in Fig. 5c presents a ΔG° trend with a positive slope and it intersects the x axis at around 800 K, highlighting that the methane decomposition starts around this temperature. The most reacting species is Fe_2O_3, starting to react at 808 K. Nevertheless, it must be taken into account that such species cannot provide a consistent contribution to the reaction yield in actual lunar soil: in fact, it is mostly present in the lunar simulants rather than in the regolith (where iron is mostly present in the form FeO).

Ilmenite ($FeTiO_3$), a core species for many different studies on ISRU, asks for a

dedicated discussion. Fig. 5b highlights that ilmenite reduction with hydrogen has always a positive ΔG°, a behavior shared with the FeO species visible in Fig. 5a. The model of the thermodynamic quantities is verified on page 155 of [31], while the standard enthalpy of formation comes from Table 2 on page 458 of [32]. This positive slope is also confirmed by the coefficients extracted from [43], page 2029, and it is further supported by [16], Table 10, in the temperature range of interest. Nevertheless, multiple sources attest that the reaction occurs, even with positive free energy. The most likely explanation is that with ΔG° larger than but close to zero, as in the cases of FeO and ilmenite, an excess of reactants (notably hydrogen) is enough to move the chemical equilibrium on the products side, even with positive free energy [15, 7, 8]. This result is also experimentally confirmed by the campaign reported in [36]: as it is recalled in Fig. 5d, the reaction is tested in the temperature range 503–1373 K with an increase of temperature of $120\,\mathrm{K\,h^{-1}}$, and the reaction starts at relatively low temperatures. The three curves correspond to different samples of ilmenite containing a TiO_2 content from 55.6 to 71.5 wt% and a different distribution of the FeO/Fe_2O_3 concentrations (Fe_{tot} 14.5-28.2 wt%), as it is reported in [44].

In summary, merging the thermodynamic considerations and the experimental counterpart, the species that react with hydrogen are FeO and ilmenite, plus Fe_2O_3.

5.3. Further investigation of silica reaction

Silicates constitute a major part of the lunar regolith. They are present in a wide variety of minerals, with very different reactivity levels: in the temperature range of interest, only some of them are capable of reacting. Then, the identification of the possible reaction paths leading to their reduction is not straightforward, and special attention is needed in their analysis. Table 5 reports the list of reactions analyzed in this Section, starting from the oxides constituents. The reactions of SiO_2 with the

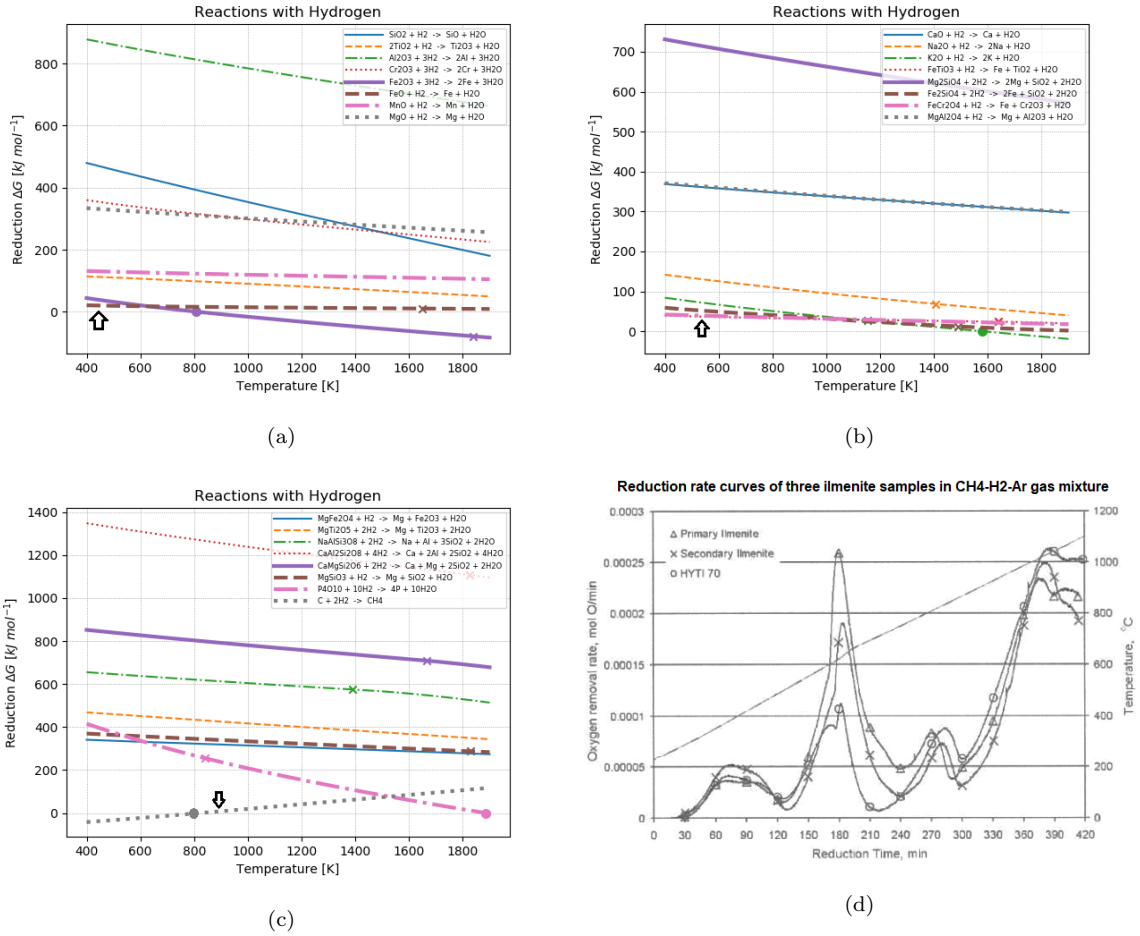

(a) (b) (c) (d)

Figure 5: **(a, b, c)**: ΔG° behavior for the different species reacting with H_2. The cross "x" marks the temperature for which a change of state occurs, the point • indicates the $\Delta G^\circ = 0$ temperature. **(d)** (reproduced from [36]): reduction rate curves for three ilmenite samples with different TiO_2 content and FeO/Fe_2O_3 proportions.

three reducing reactants and CO are included, together with SiO reactions and the equilibrium reactions CO_2 / C / CO and CH_4 / H_2 / C. Their free energy trends are reported in Fig. 6.

SiO_2 is scarcely present in pure form, but it can be obtained from several minerals. Even if oxides extraction from them can appear difficult to achieve, it must be taken into account that the temperature range here analyzed is beyond the glass transition temperature and close to the melting one for several species, and local interactions between minerals and reactants cannot be excluded. This aspect is quite complex, and proper support by experimental investigation is also needed for its correct modeling. Hence, its in-depth analysis is left for subsequent studies. Here, it is just put in evidence that some minerals are found in any case to be reactive from a thermodynamic point of view, even without considering potential additional effects due to the high temperature. Purely by way of example, *fayalite* (olivine) reacts with methane and carbon respectively at 950 K and 1046 K, following the reactions (12) and (13).

$$Fe_2SiO_{4(s)} + 2\,CH_{4(g)} \longrightarrow 2\,Fe_{(s)} + SiO_{2(s)} + 2\,CO_{(g)} + 4\,H_{2(g)} \tag{12}$$

$$Fe_2SiO_{4(s)} + 2\,C_{(s)} \longrightarrow 2\,Fe_{(s)} + SiO_{2(s)} + 2\,CO_{(g)} \tag{13}$$

The ideal situation in SiO_2 reduction - as well as for the other species - is the complete removal of the oxygen, without leaving any carbon chemically bound (e.g. when SiC is produced). This is found in the reactions forming metallic silicon, i.e. (14), (15) and (21): however, they exhibit $\Delta G^\circ = 0$ at very high temperatures. This is confirmed in [34], in which it is shown how metallic silica can be produced from a charge of Si-C-O whenever heated above 2310 K. Intermediate products, SiO and SiC, have then to be considered to explain a reaction at lower temperatures.

Table 5: Silicates reaction mechanisms with CH_4, C, H_2, CO.

SiO2-CH4 reactions		**SiO2-C reactions**	
$SiO_{2\,(s)} + 2\,CH_{4\,(g)} \longrightarrow Si_{(s)} + 2\,CO_{(g)} + 4\,H_{2\,(g)}$	(14)	$SiO_{2\,(s)} + 2\,C_{(s)} \longrightarrow Si_{(s)} + 2\,CO_{(g)}$	(15)
$SiO_{2\,(s)} + CH_{4\,(g)} \longrightarrow SiO_{(g)} + CO_{(g)} + 2\,H_{2\,(g)}$	(16)	$SiO_{2\,(s)} + C_{(s)} \longrightarrow SiO_{(g)} + CO_{(g)}$	(17)
$SiO_{2\,(s)} + 3\,CH_{4\,(g)} \longrightarrow SiC_{(s)} + 2\,CO_{(g)} + 6\,H_{2\,(g)}$	(18)	$SiO_{2\,(s)} + 3\,C_{(s)} \longrightarrow SiC_{(s)} + 2\,CO_{(g)}$	(19)
SiO2-CO reactions		**SiO2-H2 reactions**	
$SiO_{2\,(s)} + CO_{(g)} \longrightarrow SiO_{(g)} + CO_{2\,(g)}$	(20)	$SiO_{2\,(s)} + 2\,H_{2\,(g)} \longrightarrow Si_{(s)} + 2\,H_2O_{(g)}$	(21)
		$SiO_{2\,(s)} + H_{2\,(g)} \longrightarrow SiO_{(g)} + H_2O_{(g)}$	(22)
SiO reactions		**Other reactions**	
$SiO_{(g)} + 2\,C_{(s)} \longrightarrow SiC_{(s)} + CO_{(g)}$	(23)	$CO_{2\,(g)} + C_{(s)} \longrightarrow 2\,CO_{(g)}$	(24)
$SiO_{(g)} + 2\,CH_{4(g)} \longrightarrow SiC_{(s)} + CO_{(g)} + 4\,H_{2\,(g)}$	(25)	$CH_{4\,(g)} \longrightarrow 2\,H_{2\,(g)} + C_{(s)}$	(26)
$SiO_{(g)} + 3\,CO_{(g)} \longrightarrow SiC_{(s)} + 2\,CO_{2\,(g)}$	(27)		

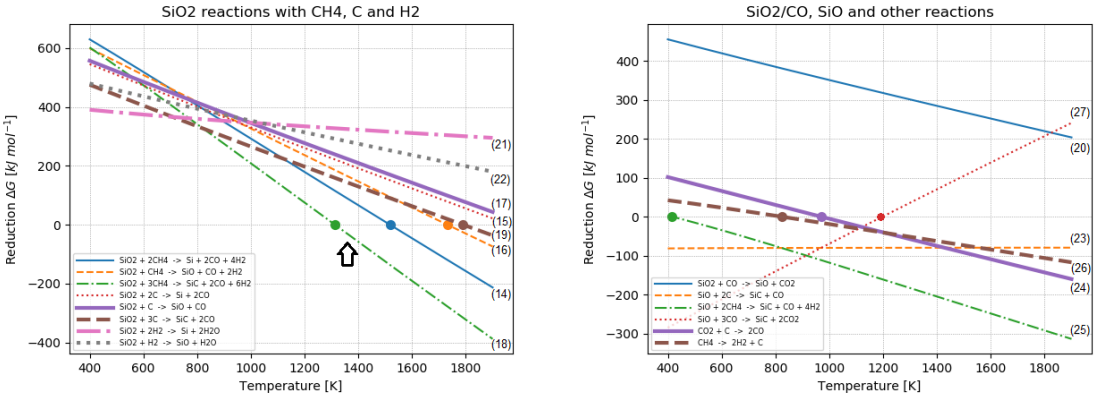

(a) (b)

Figure 6: ΔG° trend of Table 5 reactions.**(a)**: SiO_2 reactions with methane, carbon and hydrogen. **(b)**: SiO_2 reaction with CO, SiO reactions and other reactions. The point • indicates the $\Delta G^\circ = 0$ temperature.

In bibliography are presented different experimental and modeling activities carried out on SiO_2 reacting with methane, that produces the aforementioned intermediate products.

Looking at SiC, some authors [45, 24] suggest that at high temperatures SiC formation may take place in a mixture of silicates and carbon or in a methane flux, following respectively reaction (19) and (18): looking at the thermodynamics, reaction (18) can occur above 1312 K (Fig. 6a). This result finds confirmation also in [25]: it is pointed out that there is a temperature interval from about 1273 to 1773 K in which, from equilibrium considerations, the SiC production from silica oxide and methane is present. Refer to Fig. 1 in this publication, taken directly from that reference, looking at the almost linear green line in the 1000-1500 °C interval in the plot. However, there is a discrepancy between thermodynamic expectations and real experiments, that put in evidence how chemical kinetic and equilibrium among

species can have a crucial role in determining actual reactivity. This aspect comes out in [14], in which SiC formation from SiO_2 and CH_4 is observed between 1673 K and 1773 K, even if the reaction was expected below 1673 K from the thermodynamics. These same studies underline how the reaction is more likely to occur via gaseous intermediates, namely SiO.

So, considering the thermodynamic of SiO, the $\Delta G^\circ = 0$ temperatures for reactions (16) and (17) are >1750 K. Values found are in line with the results of a recent experimental study [46], that analyzed the SiO production in a fluidized bed reactor containing quartz: it was observed that the SiO production occurs mainly in the 1623–1773 K range. Furthermore, the thermodynamic investigation carried on in [14] denoted that the conditions in which methane decomposes or not have an impact on the actual reactivity. It is recalled the difference previously highlighted between the deposited carbon coming from methane cracking and the adsorbed active carbon: the higher activity of the latter has beneficial effects on the thermodynamics of the process [14].

Once $SiO_{(g)}$ is produced, the conversion to $SiC_{(s)}$ is allowed to happen in the considered temperature working range with all the reactants, as shown in Fig. 6. $SiO_{(g)}$ can be produced by reactions (16), (17), and (22), while there are three possible mechanisms (23), (25), and (27) that can produce SiC. Note that (27) after 1200 K occurs in the reverse way, as shown in Fig. 6b, and that the trend of reaction (23), negative and almost invariant with temperature, is further confirmed in [45]. Nevertheless, the production of $SiO_{(g)}$ as intermediate cannot be properly explained by simply analyzing the thermodynamics of single reactions: a path spanning multiple reactions occurring simultaneously has to be identified.

In conclusion, different factors have to be considered when trying to model the silicates reaction mechanisms: the methane decomposition/adsorption that plays a

key role in the oxygen removal mechanism; the direct SiC production mechanism that, to obtain reaction (18), passes trough (16) and (25), that summed return again (18), or the reaction paths for SiC production passing through $SiO_{(g)}$. Experimental activities will be fundamental in the formalization of a kinetic model of the process and the proper tuning of its parameters.

5.4. Further investigation on titanium reaction

Titanium oxides, and in particular ilmenite, have been widely studied for their easiness of reduction, especially with hydrogen. This property makes them an attractive target for ISRU purposes [15, 7, 8]: even if on average they are a minority among the lunar regolith constituents, specific areas in which the ilmenite fraction is up to 20 % are present [17]. One of the aims of the carbothermal reduction is to make ISRU independent on the particular landing site, targeting a wider range of minerals. Moreover, conversion efficiency of ilmenite reduction can be further increased with the addition of methane to the reactants, making the behavior of titanium oxides still worthy of further investigation in this study. Titanium has affinity with silicon and similarly reacts with oxygen, hydrogen, and carbon. Moreover, it has more probability, with respect to silicon, to form either oxides or TiC compound than the metallic form. In the lunar regolith, TiO_2 constitutes the 0.56 % of the Apollo 16 samples, taken as reference for the lunar highland soil [17].

Titanium oxide is capable to reduce directly with coke carbon:

$$TiO_{2(s)} + 3\,C_{(s)} \longrightarrow TiC_{(s)} + 2\,CO_{(g)} \tag{28}$$

However, from the results presented in Fig. 3b, with the marked orange line, this reaction occurs only after around 1550 K, above the temperature range of interest and well above the regolith melting point.

It is reported in [35] that the reduction of rutile TiO_2 is generally a complex process which entails several intermediate products, summarized by the following scheme, in which the subscript (ss) indicates a solid solution:

$$TiO_2 \longrightarrow Ti_5O_9 \longrightarrow Ti_4O_7 \longrightarrow Ti_3O_5 \longrightarrow Ti_2O_3 \longrightarrow (TiC + TiO)_{(ss)} \quad (29)$$

Reactions not detailed here: please refer to [35] for a complete explanation. The first two steps occur quickly, while the process bottleneck is the Ti_2O_3 generation, that tends to block the subsequent step until its completion, and the final conversion in titanium carbide and titanium(II) oxide. This final stage of the reduction process, from Ti_2O_3 to the production of TiO-TiC, is described by the reaction:

$$\frac{1}{2}\,Ti_2O_3 + (\frac{1}{2} + 2x)CH_4 \longrightarrow x\,TiC + (1-x)TiO + (\frac{1}{2} + x)CO + (1 + 4x)H_2 \quad (30)$$

where the fraction x of TiC depends on the reactants relative composition, according to Fig. 7. The equilibrium of the TiC-TiO species is governed by:

$$TiO + 2\,CH_4 \longleftrightarrow TiC + CO + 4\,H_2 \quad (31)$$

The TiO_2 reduction process with methane is then summarized by:

$$TiO_2 + CH_4 \longrightarrow TiO + CO + 2\,H_2 \quad (32)$$

$$TiO_2 + 3\,CH_4 \longrightarrow TiC + 2\,CO + 6\,H_2 \quad (33)$$

where (32) represents the equilibrium shifted to TiO, when $x = 0$ in (30), while (33) is the opposite condition, so $x = 1$ and TiC is maximum.

TiO_2 reduction with hydrogen is described by:

$$2\,TiO_2 + H_2 \longrightarrow Ti_2O_3 + H_2O \quad (34)$$

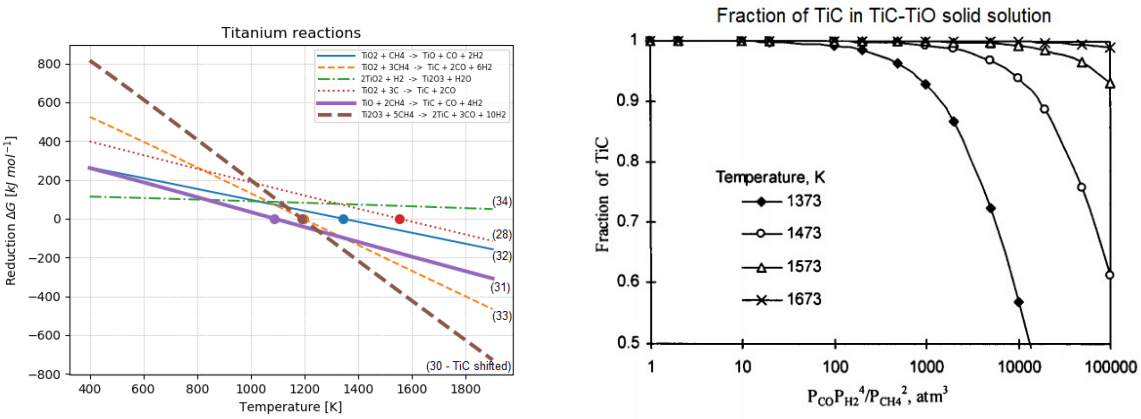

(a) (b)

Figure 7: **(a)** ΔG behavior for the Ti reactions. (30) is fully shifted to TiC product. **(b)** fraction of TiC in TiC-TiO solid solution is function of the reducing gas composition (reproduced from [35]).

At first sight, from the ΔG° trend in Fig. 7a, the reaction could not occur in the temperature range of interest. It has a positive ΔG° for all temperatures, that is also higher than the one of FeO and ilmenite, limiting the effectiveness of the principle explained in Sec. 5.2.

The reduction of each mole of TiO_2 to TiO produces one mole of CO (32), followed a second mole of CO coming from the passage from TiO to TiC (31). Figure 7a shows the ΔG° trends for these reaction mechanisms, and except the reaction with C and H_2, they all occur below the upper bound temperature 1373 K. The final equilibrium between TiC and TiO depends on the achieved gas composition, given a process temperature, and its trend is shown in Fig. 7b. It can be seen how the extraction of the oxygen can be maximized by operating in excess of reactants, a condition easily achievable when operating in a flowing gas condition.

Table 6: Yield evaluation from thermodynamic considerations. Species masses are retrieved from Table 3. As in the original data, the total mass is not exactly 1000 g due to the averaging process on the samples.

		Apollo 11		Apollo 14		Apollo 16	
Species	**Yield [%]**	**Species mass in 1000 g [g]**	**O_2 extracted [g]**	**Species mass in 1000 g [g]**	**O_2 extracted [g]**	**Species mass in 1000 g [g]**	**O_2 extracted [g]**
SiO_2	4.45	422.0	10.00	481	11.40	450.9	10.69
TiO_2	100	78.0	31.25	17	6.81	5.6	2.24
Al_2O_3	0	136.0	0	174	0	271.8	0
Cr_2O_3	100	3.0	0.95	2.3	0.73	1.1	0.35
FeO	100	153	34.07	104	23.16	51.8	11.54
MnO	100	2	0.45	1.4	0.32	0.7	0.15
MgO	0	78	0	94	0	58.4	0
CaO	0	119.0	0	107	0	157.9	0
Na_2O	100	4.7	1.21	7	1.81	4.7	1.21
K_2O	100	1.6	0.27	5.5	0.93	1.1	0.19
P_2O_5	100	0.5	0.28	5.1	2.87	1.2	0.68
O_2 extracted [g]			78.49		48.03		27.04

5.5. Preliminary yield estimation

Even if thermodynamics alone cannot give a complete picture of the reduction process yield, the contribution that different species give in terms of oxygen extracted from regolith through a carbothermal reduction can be preliminarily estimated. The three soils presented in Section 2 are taken as reference: Apollo 11 for a high-Ti basalt; Apollo 14 and Apollo 16 for, respectively, a mare basalt and a lunar highland.

Results are summarized in Table 6. The relative composition of the samples derive from Table 3: the summation of the reported masses can be slightly different from the nominal batch size 1000 g due to the samples averaging process reported in the original references.

For each species, a yield value is reported, intended as the mass fraction of the species actually reacting. For all the species found to be reactive from the thermodynamics analyzed in the previous sections, the assumed yield is 100 %, except for

the silicates. As explained in Section 5.3, reactivity among silicate minerals varies largely depending on several factors and multiple reaction paths, and only a fraction of them actually reacts. A preliminary value of 4.45 % has been obtained as yield for silicates bulk by thermogravimetric analysis carried out at Politecnico di Milano, performed on NU-LHT-2M samples with a methane/hydrogen flow (at 1/1 molar ratio) mixture at 1273 K. This value should be considered a first estimation of the reactivity of silicates, but representative of the expected order of magnitude. It was obtained in a larger experimental campaign carried on during an European Space Agency study in 2010 and used for the design of a terrestrial demonstrator [47]. This work constitutes the related theoretical counterpart, fundamental to understand the results obtained with the experiments.

Finally, for each reacting species the corresponding mass of oxygen extractable through carbothermal reduction is reported in the table.

The global yield, intended as the ratio between the total mass of extracted oxygen and the mass of the feedstock batch, ranges from 2.4 % to 7.9 %. These values correspond to 5.4 % to 17.5 % of the total available oxygen, which constitutes about 45 % of the lunar regolith (Section 2.2). The inclusion of methane in the reactants enables oxygen production in areas in which ilmenite presence is marginal, such as the lunar highlands.

It has however to be pointed out that these values are still conservative. Due to the variety of factors involved, proper tuning of reaction parameters like inlet mixture, flow rates, temperature, batch size and granulometry, time, etc. appears to leave room for further optimization of the silicate minerals yield.

6. Conclusion

This paper reports about a step forward in the production of oxygen from lunar regolith in solid phase by carbothermal reduction. The thermodynamics of the reactions between the main regolith constituents and the reducing gases CH_4 and H_2 is modeled to identify the subset of the reacting species in the 1273–1373 K temperature range, which avoids feedstock melting.

The following species have been found capable to react in the considered range, including also the species that have a ΔG° that is positive, but close to zero, and for which an experimental verification is present in bibliography:

- Reaction with H_2: Fe_2O_3, FeO, and $FeTiO_3$ (ilmenite).
- Reaction with CH_4: Fe_2O_3, FeO, TiO_2, Cr_2O_3, MnO, Na_2O, K_2O, P_4O_{10}, SiO_2 and the minerals Fe_2SiO_4 (fayalite - olivine), $FeTiO_3$ (ilmenite), $FeCr_2O_4$ (chromite - spinel).
- Reaction with C: Fe_2O_3, FeO, K_2O, P_4O_{10}, and the minerals Fe_2SiO_4 (fayalite - olivine), $FeTiO_3$ (ilmenite), $FeCr_2O_4$ (chromite – spinel).

Particular attention is given to the SiO_2 reaction mechanisms, crucial as it is the most abundant species on the Moon. Viable reduction paths are proposed for this large family of compounds, found to be partially reactive, making accessible almost all of the lunar surface. The reduction process of the titanium oxides is analyzed in detail as well, for its interest in the ilmenite reduction research. It was found that the TiO_2 reactivity with methane is high, achieving a higher oxygen extraction efficiency with respect to reduction with hydrogen. Based on the aforementioned analysis, a preliminary estimation of the expected total theoretical yield is finally presented. It is shown how the major contribute is expected to be given by the ferrous species,

followed by silicates. A preliminary, theoretical yield value (oxygen/feedstock, mass ratio) from 2.4 % to 7.9 % is estimated for the carbothermal reduction process, depending on the composition of the specific lunar locality.

Such preliminary values constitute a reliable first estimation, to be revisited upon the formulation of the process kinetics. In fact, reaction velocities and equilibrium between reactants are still to be properly modeled, supported by a solid experimental campaign. The work carried out confirms the solid-gas carbothermal reduction effectiveness as a valid candidate process for ISRU on the Moon, and opens the door to possible future demonstration with pilot plants, both in laboratory and on the lunar surface.

Acknowledgements

This work was developed in the framework contract of ASI-PoliMi Ricerca e Innovazione n.2018-H.0. funded by the Italian Space Agency.

References

[1] M. Baldry, N. Gurieff, D. Keogh, Imagining sustainable human ecosystems with power-to-x in-situ resource utilisation technology, Acta Astronaut. 192 (2022) 190–198.

[2] N. Kalapodis, G. Kampas, O.-J. Ktenidou, A review towards the design of extraterrestrial structures: From regolith to human outposts, Acta Astronaut. 175 (2020) 540 – 569.

[3] D. B. Stoeser, D. L. Rickman, S. A. Wilson, Design and Specifications for the Highland Regolith Prototype Simulants NU-LHT-1M and -2M, NASA/TM 2010-216438.

[4] G. Cesaretti, E. Dini, X. De Kestelier, V. Colla, L. Pambaguian, Building components for an outpost on the Lunar soil by means of a novel 3D printing technology, Acta Astronaut. 93 (2014) 430 – 450.

[5] E. Stoll, P. Härke, S. Linke, F. Heeg, S. May, The regolith rocket — A hybrid rocket using lunar resources, Acta Astronaut. 179 (2021) 509 – 518.

[6] D. L. Linne, S. Nozette, M. Downey, D. McKay, R. L. Johnson, E. McCullough, L. Martin, R. M. Zubrin, L. S. Gertsch, In-Situ Resource Utilization (ISRU) Capability Roadmap - Final Report (2005) 2–8.

[7] D. Kaschubek, M. Killian, L. Grill, system analysis of a moon base at the south pole: considering landing sites, eclss and isru, Acta Astronaut. 186 (2021) 33–49.

[8] L. A. Taylor, W. D. Carrier III, Production of Oxygen on the Moon: Which Processes Are Best and Why, AIAA J. 30 (12) (December 1992) 2858–2863.

[9] C. Schwandt, J. A. Hamilton, D. J. Fray, I. A. Crawford, The production of oxygen and metal from lunar regolith, Planet. Space Sci. 74 (1) (December 2012) 49–56.

[10] R. J. Gustafson, B. C. White, M. J. Fidler, A. C. Muscatello, Demonstrating the Solar Carbothermal Reduction of Lunar Regolith to Produce Oxygen, 48th AIAA Aerospace Sciences Meeting Including the New Horizons Forum and Aerospace Exposition, 4 - 7 January 2010, Orlando, Florida, AIAA 2010-1163 (2010) 4–12.

[11] A. Goulas, J. G. Binner, R. A. Harris, R. J. Friel, Assessing extraterrestrial regolith material simulants for in-situ resource utilisation based 3D printing, Appl. Mater. Today 6 (2017) 54–61.

[12] S. S. Schreiner, J. A. Dominguez, L. Sibille, J. A. Hoffman, Thermophysical property models for lunar regolith, Adv. Space Res. 57 (5) (2016) 1209–1222.

[13] C. Alba-Simionesco, J. Fan, C. A. Angell, Thermodynamic aspects of the glass transition phenomenon. II. Molecular liquids with variable interactions, Chem. Phys. 110 (1999) 5262–5272.

[14] M. Ksiazec, M. Tangstad, H. Dalaker, E. Ringdalen, Reduction of SiO2 to SiC Using Natural Gas, Metall. Mater. Trans. E 1 (3) (September 2014) 272–279.

[15] H. Sargeant, S. Barber, M. Anand, F. Abernethy, S. Sheridan, I. Wright, A. Morse, Hydrogen reduction of lunar samples in a static system for a water production demonstration on the Moon, Planet. Space Sci. 205 (2021) 105287.

[16] C. Shomate, B. Naylor, F. Boericke, Thermodynamic Properties of Ilmenite and Selective Reduction of Iron in Ilmenite, [Washington, D.C.]: U.S. Dept. of the Interior, Bureau of Mines, R.I. 3864 (1946) 1–20.

[17] G. Heiken, D. Vaniman, B. French, Lunar Sourcebook: A user's guide to the Moon, Chapter 5, C. U. P. (1991) 121–182.

[18] B. A. Lomax, M. Conti, N. Khan, N. S. Bennett, A. Y. Ganin, M. D. Symes, Proving the viability of an electrochemical process for the simultaneous extraction of oxygen and production of metal alloys from lunar regolith, Planet. Space Sci. 180 (2020) 104748.

[19] A. Meurisse, B. Lomax, Áron Selmeci, M. Conti, R. Lindner, A. Makaya, M. D. Symes, J. Carpenter, Lower temperature electrochemical reduction of lunar regolith simulants in molten salts, Planet. Space Sci 211 (2022) 105408.

[20] G. Heiken, D. Vaniman, B. French, Lunar Sourcebook: A user's guide to the Moon, Chapter 7, C. U. P. (1991) 283–356.

[21] L. Sibille, P. Carpenter, R. Schlagheck, R. A. French, Lunar Regolith Simulant Materials: Recommendations for Standardization, Production and Usage, NASA/TP—2006–214605 (2006) 6–13.

[22] P. J. Guichelaar, Acheson Process, Carbide, Nitride and Boride Materials Synthesis and Processing, Chapman & Hall Chapter 4 (1997) 115–129.

[23] R. Balasubramaniam, S. Gokoglu, U. Hegde, The reduction of lunar regolith by carbothermal processing using methane, Int. J. Miner. Process. 96 (2010) 54–61.

[24] K. Wiik, K. Motzfeldt, Kinetics of reactions between silica and carbon and the formation of silica carbide, MRS OPL 410 (1995) 435–440.

[25] H.-C. Lee, S. Dhage, M. S. Akhtar, D. H. Kwak, W. J. Lee, C.-Y. Kim, O.-B. Yang, A simulation study on the direct carbothermal reduction of SiO2 for Si metal, Curr. Appl. Phys. 10 (2, Supplement) (2010) S218–S221, the Proceeding of the International Renewable Energy Conference and Exhibition 2008 (RE2008).

[26] H. Uchinda, M. R. Harada, Chapter 5.3.3 - Application of Hydrogen by Use of Chemical Reactions of Hydrogen and Carbon Dioxide, in: P. E. V. de Miranda (Ed.), Science and Engineering of Hydrogen-Based Energy Technologies, Academic Press, 2019, pp. 279–289.

[27] S. Gordon, B. McBride, Computer program for calculation of complex chemical equilibrium compositions and applications - Part I. Analysis, NASA Tech. Rep. RP-1311 (1994) 31–32.

[28] S. Gordon, B. McBride, Computer program for calculation of complex chemical equilibrium compositions and applications - Part II. Users Manual and Program Description, NASA Tech. Rep. RP-1311 (1994) 73–94.

[29] NASA, NASA Chemical Equilibrium with Applications (CEA), (last access 31/05/2022).

[30] NIST, NIST Chemistry WebBook, SRD 69, (last access 31/05/2022).

[31] R. A. Robie, B. S. Waldbaum, Thermodynamic Properties of Minerals and Related Substances at 298.15°K (25.0°C) and One Atmosphere (1.013 Bars) Pressure and at Higher Temperatures, Geol. Survey Bull. (1259) (1968) 1–234.

[32] R. G. Berman, Internally-Consistent Thermodynamic Data for Minerals in the System Na2O-K2O-CaO-MgO-FeO-Fe2O3-Al2O3-SiO2-TiO2-H2O-CO2, J. Petrol. 29 (2) (1988) 445–522.

[33] A. Tsutsumi, Thermodynamics of water splitting, Energy carriers and conversion systems, Edited by Tokio Ohta, Encyclopedia of Life Support Systems (EOLSS) Vol. 1 (ISBN: 9781905839292).

[34] M. Nagamori, I. Malinsky, A. Claveau, Thermodynamics of the Si-C-O System for the Production of Silicon Carbide and Metallic Silicon, Metall. Trans. B 17 (1986) 503–514.

[35] G. Zhang, Reduction of Rutile and Ilmenite by Methane-Hydrogen Gas Mixture, A thesis in Materials and Metallurgical Engineering, The University of New South Wales Faculty of Science and Technology School of Materials Science and Engineering (March 2000) 76–85, 93, 135–139.

[36] G. Zhang, O. Ostrovski, Reduction of Ilmenite Concentrates By Methane Containing Gas, Part II: Effects of Preoxidation and Sintering, Can. Metall. Q. 40 (4) (October 2001) 489–498.

[37] J. Pan, S. Li, D. Zhu, J. Xu, J. Chou, Migration of Iron, Aluminum and Alkali Metal Within Pre-reduced-Smelting Separation of Bauxite Residue, Light Metals 2019 (Chesonis, Corleen) (2019) 107–111.

[38] A. Navrotsky, Thermodynamics of Formation of Some Compounds with the Pseudobrookite-Structure and of the FeTi2O5-Ti3O5 Solid Solution Series, Am. Min. 60 (1975) 249–256.

[39] K. Charan Sabat, Reduction of Oxide Minerals by Hydrogen Plasma: An Overview, Plasma Chem. Plasma Process 34 (1) (January 2014) 1–23.

[40] I. V. Ryabchikov, B. F. Belov, V. G. Mizin, Reactions of metal oxides with carbon, Steel Transl. 4 (2014) 368–373.

[41] D. M. Burt, Lunar mining of oxygen using fluorine, The Second Conference on Lunar Bases and Space Activities of the 21st Century, NASA-CP 3166 (1988) 423–428.

[42] X. Li, G. Zhang, K. Tang, O. Ostrovski, R. Tronstad, Carbothermal reduction of quartz in methane-hydrogen-argon gas mixture, Metall. Mater. Trans. B 46 (5) (2015) 2384–2393.

[43] L. M. Anovitz, A. H. Treiman, E. J. Essene, B. S. Hemingway, E. F. Westrum, V. J. Wall, R. Burriel, S. R. Bohlen, The heat-capacity of ilmenite and phase equilibria in the system Fe-Ti-O*, Geochim. Cosmochim. Acta 49 (10) (1985) 2027–2040.

[44] G. Zhang, O. Ostrovski, Reduction of Ilmenite Concentrates By Methane-containing Gas: Part I. Effects of Ilmenite Composition, Temperature and Gas Composition, Can. Metall. Q. 40 (3) (2001) 317–326.

[45] Gmelin-Institut fUr Anorganische Chemie der Max-Planck-Gesellschaft zur Forderung der Wissenschaften, Gmelin Handbook of Inorganic Chemistry - 8th edition, Springer-Verlag Berlin Heidelberg GmbH (1986) 51–71.

[46] X. Li, G. Zhang, K. Tang, O. Ostrovski, R. Tronstad, Reduction of Quartz to Silicon Monoxide by Methane-Hydrogen Mixtures, Metall. Mater. Trans. B 47 (April 2016) 2197–2204.

[47] A. Colagrossi, C. Contini, M. Lavagna, P. Lunghi, J. Prinetto, F. Scala, Lunar ISRU Demonstrator Technology: Demonstrator Description Document, Politecnico di Milano, ISRU-DEMO-DD-DPMT (Issue 1, Rev 4, 09/04/2019) (Unpublished results) 11–24.